RSC Advances

ROYAL SOCIETY OF CHEMISTRY

www.rsc.org/advances

Grain size dependent magnetoelectric coupling of $BaTiO_3$ nanoparticles

Tesfakiros Woldu[1,2], B. Raneesh[3], M.V. Ramana Reddy[1], Nandakumar Kalarikkal[4,5*]

[1]Department of Physics, Osmania University, Hyderabad 500 007, Telangana, India
[2]Department of Physics, Mekelle University, Mekelle, Tigray, Ethiopia
[3]Department of Physics, Catholicate College, Pathanamthitta, 689 645, Kerala, India
[4]International and Interuniversity Centre for Nanosciecne and Nanotechnology, Mahatma Gandhi University Kottayam 686 560, Kerala, India
[5]School of Pure and Applied Physics, Mahatma Gandhi University, Kottayam 686 560, Kerala, India

Abstract:

We report magneto-electric (ME) coupling property of $BaTiO_3$ nanoparticles of different grain sizes ranging from 16-26nm synthesized by a modified Pechini method. Nanostructured multiferroic $BaTiO_3$ shows good ferroelectric and magnetic properties at room remperature, which is confirmed by temperature dependent dielectric spectroscopy and magnetometer. A quantitative magneto-electric coefficient measurement in $BaTiO_3$ samples at room temperature was performed using the dynamic lock-in amplifier technique. The obtained magnetoelectric coefficient value of all the samples indicate the occurrence of strong magneto-electric coupling and the maximum recorded at AC magnetic field of 77 Oe is 32 mV/cmOe and exhibits size-dependent magnetoelectric coupling. This enhanced room temperature ME voltage coefficient with perfect ME anisotropy provides a possibility of using such a material in low energy consumption for miniaturized device applications in the area of sensors and memory devices.

Keywords: Ferroelectric, Ferromagnetic, Multiferroic, Magnetoelectric coupling

E-mail: nkkalarikkal@mgu.ac.in, Tel: +919447671962, Fax: +91481-2731669, Mail address: School of Pure and Applied Physics, Mahatma Gandhi University, Kottayam, Kerala 686 560, India

1. INTRODUCTION

The coexistence of several order parameters in MF brings out novel physical phenomenon and offers a possibility for new device functionalities.[1-4] The current surge of interest in MF materials showing magnetoelectric (ME) coupling due to the presence of both magnetic and ferroelectric ordering is fuelled by both the potential technological applications and the underlying new physics.[5-8] The coexistence of magnetic and ferroelectric ordering only is not enough; of the most importance is to require strong coupling interaction between two ferroic (FM, FE) orders, [9-11] because of the possibility of controlling magnetization or magnetic order by electric field[12-16] , and ferroelectric polarization by magnetic field.[15] Magnetization and polarization could independently encode information in a single MF bit, and coupling of them in principle could permit data to be written electrically, and read magnetically.[7]

Ferroelectric or antiferromagnetic/ferromagnetic properties are the general prerequisites for compounds to induce ME coupling. However, there are few[17, 18] MF systems existing in nature at room temperature because transition metal d electrons reduce the tendency for an off-centering FE distortion.[19] Due to this rareness of single phase MF material that exhibits coupling of ferroelectricity with ferromagnetism has then led many researchers to combine ferroelectric materials with ferromagnetic phases at nanoscopic scales.[12, 16,20]. For example, spin-polarization of Fe/ and Co/$BaTiO_3$ interfaces were controlled by the direction of ferroelectric polarization in $BaTiO_3$, and detected for both cases a spontaneous and hysteresis magnetic moment in $BaTiO_3$.[21, 22] So far, only hexaferrites have shown sizable control of ferroelectric polarization by magnetic field.[23]

Recent reports confirm the occurrence of magneto-electric coupling in a single phase hexagonal nanocrystalline $YMnO_3$ at low temperature.[24] $BaTiO_3$ has been one of widely used indispensable compounds as a composite multiferroic material. To achieve atomic level ME coupling in ferromagnetic $BaTiO_3$, chemical synthesis would be a good choice in order to obtain the pure phase than the conventional solid state reaction method.[25] The extraction of multiferroic and magnetoelectric effect of nanocrystalline $BaTiO_3$ motivates us to investigate magneto-electric coupling effect of different samples of nanocrystalline $BaTiO_3$ prepared by polymer precursor method. A total of ten samples of $BaTiO_3$ nanoparticles were synthesized by varying citric acid to ethylene glycol ratio in the citrate solutions from 10-50% under the same heat

treatment. In this paper, we explore the magneto-electric effect of different nanocrystalline $BaTiO_3$ samples employing the dynamic lock-in amplifier technique.

2. EXPERIMENTAL

2.1 Materials

Barium titanate powder was prepared by complex method based on the Pechini type reaction route[26] by mixing barium and titanium citrates. The chemicals used are barium acetate $Ba[C_2H_3O_2]_2$ (Sigma Aldrich 99%) , titanium-tetra isopropoxide Ti $[OCH(CH_3)]_4$ (Sigma Aldrich, $\geq$ 97%), citric acid $C_6H_8O_7$ (Merck) and ethylene glycol $C_2H_6O_2$ (Merck).

2.2 Synthesis

Barium citrate solution was prepared by dissolving barium acetate $Ba[C_2H_3O_2]_2$ (Sigma Aldrich 99%) in citric acid $C_6H_8O_7$ solution then the solution was heated at 90 ^{0}C and when it becomes transparent, ethylene glycol $C_2H_6O_2$ (Merck) was added. Parallel to this a titanium citrate solution was prepared by dissolving titanium-tetra isopropoxide Ti $[OCH(CH_3)]_4$ (Sigma Aldrich, $\geq$ 97%) in a solution of ethylene glycol at T > 60 ^{0}C with constant stirring for 10min. Then the citric acid solution was added. Solutions of barium citrate and titanium citrate were mixed, at 90 ^{0}C with constant stirring until it became clear transparent yellow solution. The temperature was maintained in the range 120 ^{0}C – 140 ^{0}C, to promote polymerization and remove solvents. The solution became more viscous and its color changes from light yellow to brown and finally solidifies into a dark brown glassy resin. Decomposition of most of the organic part was performed in an oven at 250 ^{0}C for 1hr, and then at 300 ^{0}C for 4hrs. The resin became a bulk solid mass, and then the material was pulverized, using Agate Mortar and Pestle, before further treatment. Thermal treatment was performed at 500^{0}C for 4hrs, 700 ^{0}C for 3hrs, and 750 ^{0}C for 2hrs. The agglomerates were broken in Agate Mortar, and then BTO powder was obtained. Finally, further heat treatment was carried out at a temperature of 850 ^{0}C, 950 ^{0}C, 1050 ^{0}C, and 1150 ^{0}C for the sample synthesized using 25% CA. After drying the samples at room-temperature, the agglomerates were broken in Agate Mortar and finally the BTO powder was obtained. More detail of the experimental procedure are described elsewhere.[26] The measurement values of each sample is recorded and then listed in Table 1.

Table I. Sample code, CA percentage, calcinations temperature, average grain size and linear magnetoelectric coupling coefficient (α) of respective $BaTiO_3$ samples.

Sample code	CA percentage	Calcinations Temp. (^{0}C)	Average Grain Size (nm)	α (mV/cmOe)
BT-1	10	750	25	15
BT-2	20	750	18	23
BT-3	25	750	16	32
BT-4	30	750	21	16
BT-5	40	750	24	16
BT-6	50	750	26	12
BT-A	25	850	20	18
BT-B	25	950	21	14
BT-C	25	1050	22	13
BT-D	25	1150	23	11

3. RESULTS AND DISCUSSION

3.1 Structural and morphological characterization

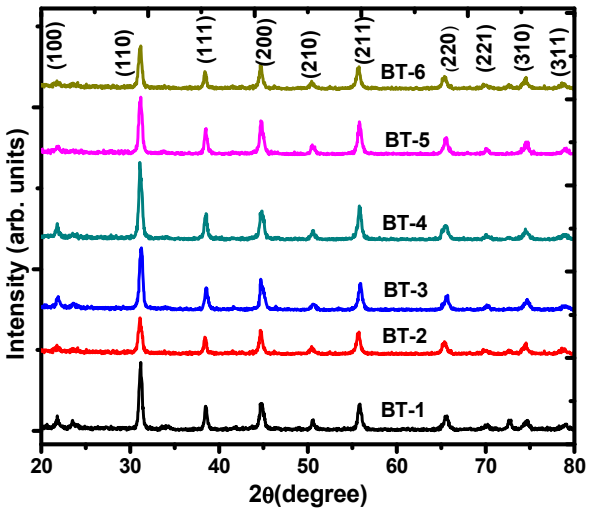

Fig. 1: XRD patterns of $BaTiO_3$ samples obtained by varying CA percentage

The structural characterization of the samples was carried out using X-ray diffractometer (PANalytical, X'Pert PRO) with a monochromatized CuK_α radiation. Fig. 1 shows XRD patterns

of six samples obtained by heating/calcining all samples at 750 ^{0}C which were prepared by varying CA concentration 10 - 50%. The XRD patterns obtained from all the samples are in correlation with the diffraction peak positions and intensities and in agreement with the structure reported in JCPDS files no. 31-0174 of known $BaTiO_3$ crystalline phases with cubic structure. Grain size of each sample was estimated from four higher intensity averaged XRD peaks by using Scherrer formula and was found to be in the range between 16-26nm and is listed in Table 1.

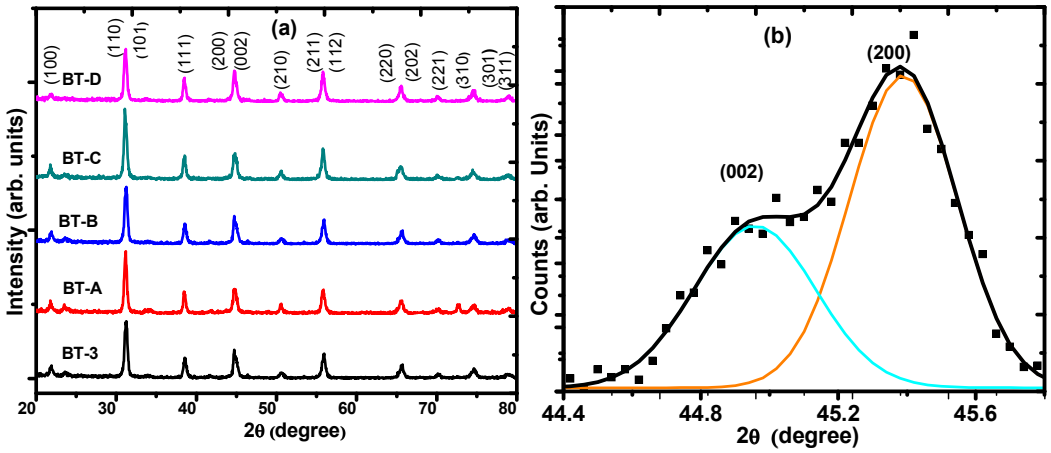

Fig. 2: XRD pattern of $BaTiO_3$ samples (a) with heat-treatment at different temperatures, and (b) XRD pattern of BT-3 splitting peak (200) and (002) at around $2\theta = 45^0$.

Fig. 2(a) shows XRD patterns of samples prepared by the same CA concentration (25%), but calcined at different temperatures, ranging from 750 ^{0}C - 1150 ^{0}C. The XRD patterns of BT-3, BT-A, and BT-B samples reveal crystalline phase of $BaTiO_3$ with cubic structure, but the XRD pattern obtained for BT-C, and BT-D samples; peak (110) and (101) around $2\theta = 31.5^0$, peak (200) and (002) around $2\theta = 45^0$; shows splitting. Fig. 2(b) shows the split of peak (200) and (002) at around $2\theta = 45^0$, this reveals the formation of tetragonal phase of $BaTiO_3$, which are the strongest, that correspond to tetragonal planes of $BaTiO_3$ in correlation with structure reported in JCPDS file no. 5-0626. Fig. 2(b) provides evidence for the formation of the unit cell of $BaTiO_3$ from cubic to tetragonal. Increasing calcination temperature between 1050 ^{0}C - 1150 ^{0}C is demonstrated by cubic to tetragonal phase transition. The estimated grain sizes using the same technique carried out above was found to be in the range 16-23 nm and is listed in Table 1.

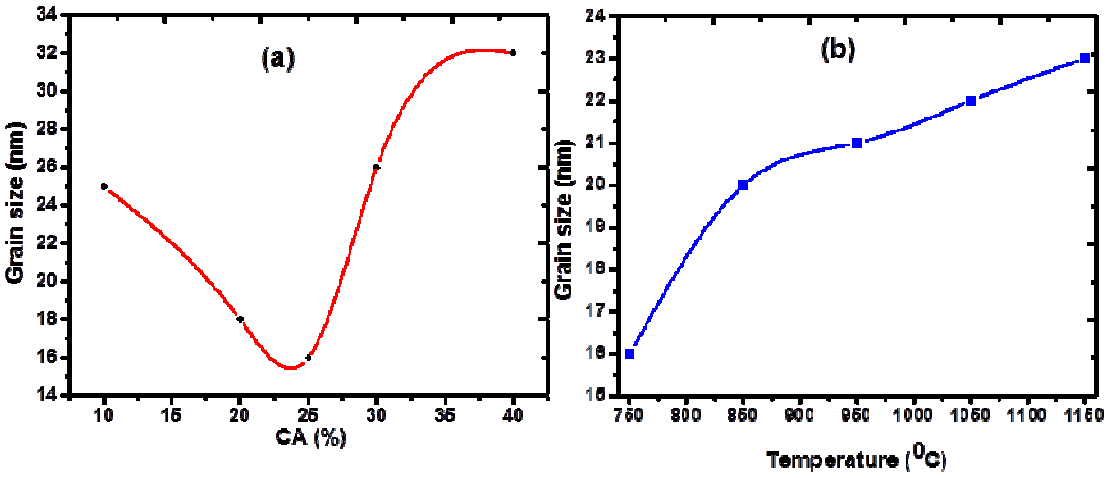

Fig. 3: (a) Grain size versus citric acid percentage and (b) Grain size vs. temperature

Fig. 3(a) shows grain size verses CA% of BT-1 to BT-6 samples. Grain size of each sample was estimated from four higher intensity averaged XRD peaks by using Scherer formula and was found to be in the range between 16-26 nm. The smaller grain size obtained was 16 nm; this is because of stronger bonding which is resulted due to good polymerization. Below or above 25% of CA, grain size increased. The time taken for polymerization for samples prepared by less than 25% CA was longer and shorter for samples prepared above 25% CA. Variation of polymerization time may account for the occurrence of this week bonding that resulted for a bigger grain size. Fig. 3(b) shows temperature dependence of grain size as calcinations temperature increases grain size increases samples synthesized by the same CA to EG ratio.

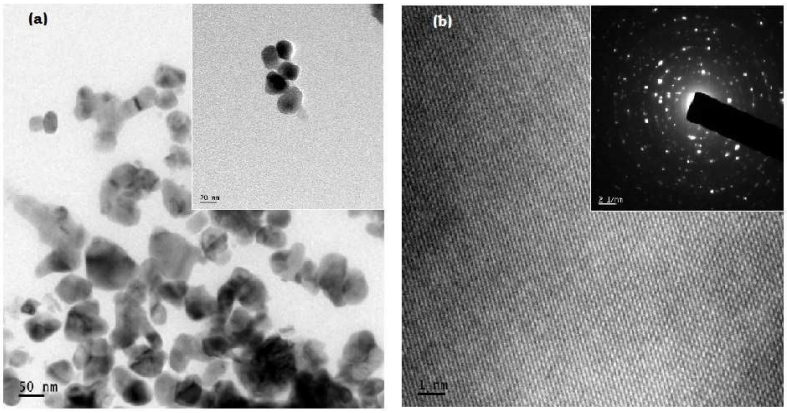

Fig. 4: (a) TEM image of sample BT-3, the inset shows 20 nm $BaTiO_3$ nanoparticles, and (b) Lattice image and the inset is a SAED pattern

Micro-structural analysis, particle size and morphology were investigated using images of high resolution transmission electron microscope (HRTEM), JEOL-JEM 2100 operating at 200kV. The TEM image in Fig. 4(a) shows some agglomerates of $BaTiO_3$ nanoparticles of sample BT-C and the particles shown in the insert are spherical nanoparticles of size 20 nm. The sizes of the synthesized $BaTiO_3$ nanoparticles are between 10-35 nm and are in spherical shape, where as the estimated average grain size of $BaTiO_3$ samples from the XRD result are in the range between 16-26 nm. This varying size of the individual particle suggests that synthesized samples are found to be polycrystalline. Fig. 4(b) shows a typical lattice image of a 20 nm nanocrystalline grain with a clear lattice fringes having d-spacing of 0.25 nm and reveals the formation of well-crystalline BT nanoparticles. The inset in Fig. 4(b) shows image of the geometry of selected area electron diffraction (SAED). The circular bright rings in SAED pattern indicate particles of barium titanate were nano crystalline in nature.

To study phase transitions Raman measurements were performed at room temperature using the Jobin-Yvon T64000 triple spectrometer system. Raman spectroscopy is a powerful tool to investigate cubic-tetragonal phase transition by probing the structure of the $BaTiO_3$ samples. Fig. 5(a) shows the Raman spectra of $BaTiO_3$ samples synthesized by different CA concentration and while calcinations temperature maintained same, and 5(b) shows samples synthesized by same concentration of CA while calcined at different temperature. The Raman spectra for these samples have been plotted in the wave number ranging from 100 cm^{-1} to 800 cm^{-1}. In the tetragonal $BaTiO_3$, there are Raman active lattice vibration modes, but there are no Raman active modes in the cubic $BaTiO_3$.[27] Raman spectrum of the samples calcined at 1050 ^{0}C and 1150 ^{0}C exhibit the characteristic features of the $BaTiO_3$ tetragonal phase: a broad peak at about 264 cm^{-1} corresponding to [A_1 (TO)], a sharp peak at 308 cm^{-1} corresponding to [B_1 and E(TO+ LO)], an asymmetric peak at 516cm^{-1} corresponds to [A_1 (TO), and E(TO)] and the peak at 715 cm^{-1} related to [A_1 (LO) and E(LO)] phonon modes.[22] A small dip at 180 cm^{-1} and 183 cm^{-1} of respective spectra's of BT-C and BT-D are attributed to the anharmonic coupling among three A_1 (TO) phonons.[28-30] Other samples calcined below 850 ^{0}C the Raman modes at peaks at 518 cm^{-1} and 718 cm^{-1} are broadened. This broadening and reduction in the intensity of the peaks and disappearance of peak 715 cm^{-1} reveal distorted cubic structure. Fig 5(b) shows the broadening of those peaks as grain size decreases.

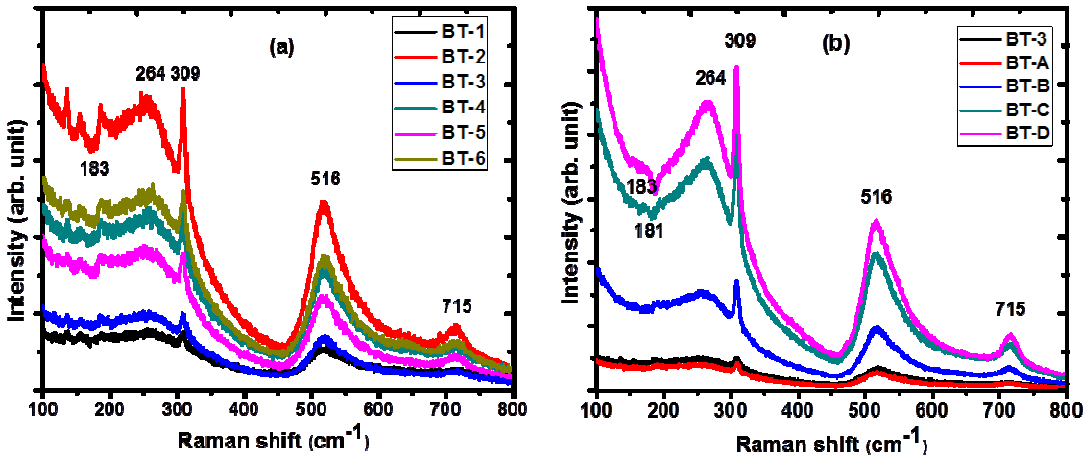

Fig. 5: Raman spectrum of (a) BT-1 to BT-6 samples, and (b) BT-3 to BT-D samples.

3.2 Ferroelectric properties

In order to confirm the Ferroelctric properties of BTO samples , The real dielectric constant ε' variation with temperature at 20 test frequencies have been measured and shown in Fig. 6. The value of ε' shows dispersion behavior with decreasing test frequencies[31]. It is observed that the dielectric constant is found to increase with temperature, reach a maximum value at Curie temperature (T_C) and after follow a decreasing trend indicating phase transition. However, the observed peak temperature, Curie temperature (T_C) is in the range between 120^0 C - 150^0 C. which is clear indication of ferroelectricity of the samples. As temperature increases the mobility of charge carriers increases which result to an increase in the polarization and conductivity of the samples, thus dielectric constant increase. The enhanced value of ε' may be ascribed: due to the space charge polarization effect at the interface of the ferrite/ferroelectric phases[32], and the hopping conduction mechanism which is thermally activated process. As temperature increases, the hopping of holes between Ba^{3+} /Ba^{2+} in ferroelectric phase give rise to p-type charge carriers[33-36]however, the contribution of p-type carriers is negligible compared to n-type carriers because their contribution decreases rapidly at low frequency. Further increase in the temperature beyond the critical temperature causes the dielectric constant of the composites to decline.

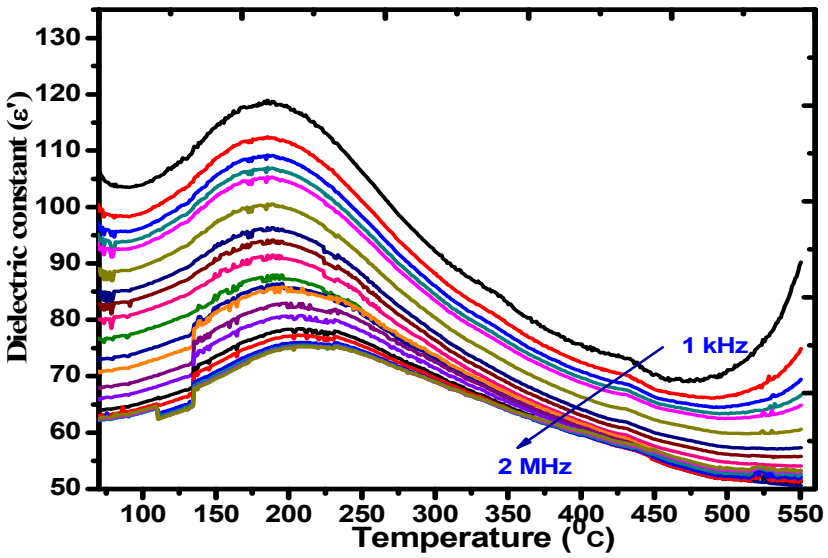

Fig. 6: Temperature dependence of dielectric constant ($\varepsilon^{'}$) of sample BT-D

3.3 Magnetic properties

In an effort to get a thorough understanding of the magnetic properties, VSM measurement was performed at room temperature for bias field of 15 kOe. Fig. 7 shows the magnetization versus magnetic field measurement of nanocrystalline $BaTiO_3$ of sample BT-D. The sample shows ferromagnetic behavior with coercive field 159 Oe, remnant magnetization $28x10^{-4}$ emu/g and saturation magnetization 1.89 x 10^{-2} emu/g. This shows the occurrence of ferromagnetism in $BaTiO_3$ nanoparticles, which was shown theoretically, that point defects such as cation/anion vacancies in insulator can create magnetic moments.[37,38] $BaTiO_3$ is a ferroelectric material but from the obtained result, one can understand ferromagnetism is intrinsic to the nanocrystalline $BaTiO_3$. [1]

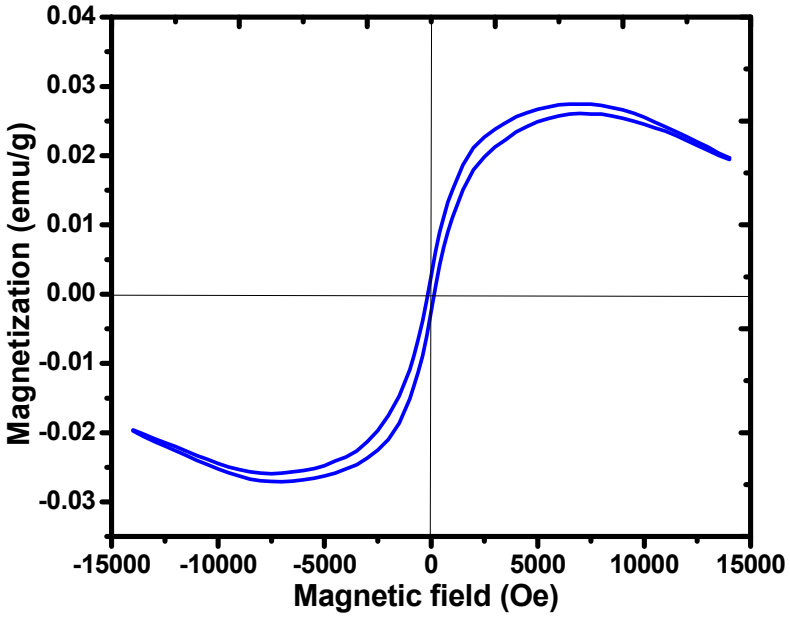

Fig. 7: Room-temperature magnetic hysteresis of sample BT-D.

3.2 ME coupling of nanocrystalline $BaTiO_3$

Magnetoelectric (ME) effect is dielectric polarization of a material in an applied magnetic field or an induced magnetization in applied external electric field. The coexistence of the ferroelectric and ferromagnetic phases in $BaTiO_3$ samples gives rise to a magnetoelectric effect , which is analyzed by the linear magnetoelectric coupling coefficient, $\alpha = dE/dH$. [39] To confirm the magnetic and electric dipole interaction at atomic level, the ME coupling coefficient of $BaTiO_3$ samples has been determined using the dynamic lock-in amplifier method since there is no any methodical review on way of measuring polarization difference of a ME nanostructured material under magnetic field. The linear ME coupling coefficient α, can be written either electrically as $\alpha_E=dM/dH$ or magnetically $\alpha_H=dP/dH$. Magnetoelectric output voltage across $BaTiO_3$ samples were measured by applying external magnetic field. In this dynamic measurement the linear ME coupling coefficient (α) is determined at a fixed DC magnetic field along with simultaneous sweeping of the AC magnetic field. Similarly, magneto electric output voltage across $BaTiO_3$ samples were recorded at fixed bias AC magnetic field along with simultaneous sweeping of the DC magnetic field. [40]

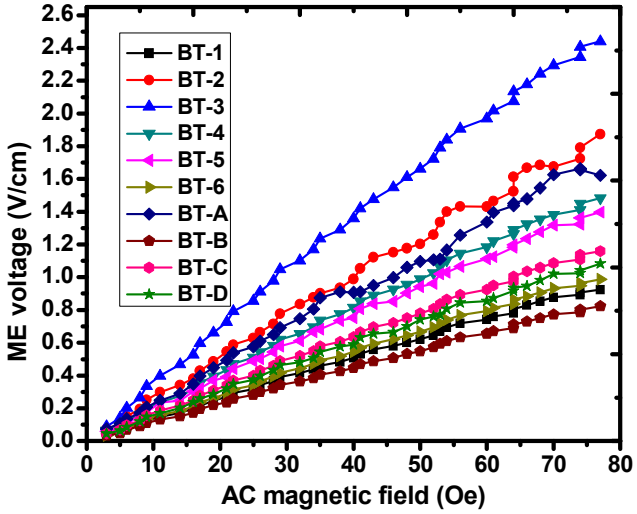

Fig. 8: ME voltage vs. AC magnetic field at constant DC (500 O e) bias magnetic field of $BaTiO_3$ samples.

Fig. 8 shows the dependence of ME voltage on AC magnetic field at room temperature. The measurements have been performed by coupling of 500 Oe DC magnetic field of frequency 850 Hz collinearly with sweeping AC magnetic field from 0 to 80 Oe. Magnetoelectric voltage response of all the $BaTiO_3$ samples shows linear path. The ME coupling coefficient (α) value of each sample was calculated from the slope of respective ME voltage versus AC magnetic field plot and recorded in Table 1. All samples show magnetoelectric effect and the maximum calculated value of linear ME coefficient was, α ~ 32mV/Oe cm. This is highest value of linear ME coefficient, compared to the reported value of same material.[41, 42] This is highly significant from technological point of view, such high value from a single phase polycrystalline compound is a promising finding for the application of new generation devices.

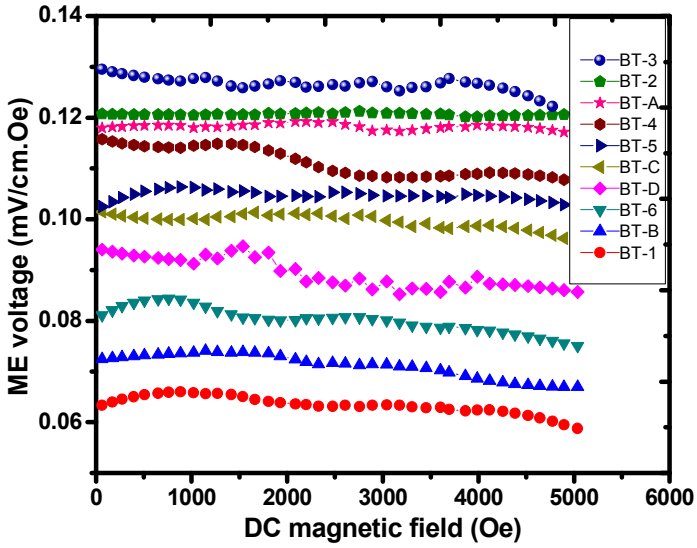

Fig. 9 ME voltage vs. DC magnetic field at constant AC (5 O e) bias magnetic field of $BaTiO_3$ samples

Fig. 9 shows the ME voltage versus DC magnetic field plot at room temperature. In this measurement, a coupling of 5 Oe AC magnetic field of 850 Hz frequency was applied collinearly with sweeping DC magnetic field from 0 to 5000 O e. The ME coupling coefficient values of $BaTiO_3$ samples calculated from the ratio of output ME voltage to applied DC magnetic field of respective samples.[41] As it is well known that the strain due to magnetostriction increases with DC magnetic field and saturates at certain field.[43] The values obtained in this measurement are in line with the values obtained for AC magnetic field sweeping measurements.

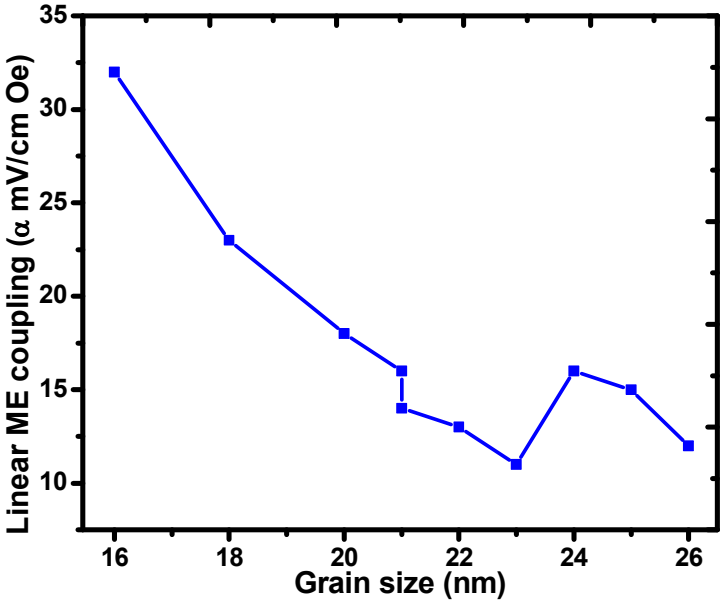

Fig.10: Linear ME coefficient vs grain size of $BaTiO_3$ samples

Fig. 10 shows linear ME coefficient versus grain size of all the $BaTiO_3$ samples ranging from 16 to 26 nm. As it is seen from the plot, linear ME coupling coefficient decreases with increasing grain size, it shows the dependence of magnetization of nanoparticles on grain size. When the grain size gets smaller and smaller, lattice size diminishes, then the surface strain[43] introduces coordinated distortion and in turn disorder permeate throughout the entire particle, as opposed to being confined only at the surface.[44] Consequently, different frustrated spin structures are produced. In addition, particle's magnetization increases, inter particle interactions become stronger. This may be attributed for the increase of linear ME coupling with decreasing grain size.

4. CONCLUSION

Nanocrystalline $BaTiO_3$ samples have been synthesized using polymer precursor method by varying citric acid to metal ion ratio and calcinations temperatures. The structural properties of synthesized samples were characterized by XRD, TEM and Raman spectroscopy. XRD and Raman spectroscopy analysis confirm the formation of pure $BaTiO_3$ nanoparticles of cubic and

tetragonal phases. The ordered ferroelectric and ferromagnetic behavior of the sample at room temperature were confirmed by variation in dielectric constant as a function temperature and M-H hysteresis loops, respectively. All the nanocrystalline $BaTiO_3$ samples show the co-existence of ferromagnetism and ferroelectricity at room temperature. The linear ME coupling coefficient values ranges from 10.7 to 32 mV/cm Oe and shows the dependence of ME coupling coefficient values on grain size of $BaTiO_3$ samples. The values are found to increase with reduction in grain size. The present investigations confirm nanosized $BaTiO_3$ as a single phase ferroelectric based magnetoelectric coupling material, and makes it a significant material for a variety of next generation device applications in the area of spintronics, sensors, memory device, and actuators.

ACKNOWLEDGEMENT

The author (TW) is thankful to Government of Ethiopia for the financial support through Osmania University, University foreign relation office (UFRO) program, Hyderabad, TS, and India. NK also acknowledges the financial support from DST-Govt. of India through the Nano Mission, PURSE, FIST Programs, and UGC-Govt. of India for the SAP program. MVR also acknowledges to UGC-UPE-FAR, OU New Delhi for providing financial assistance.

REFERENCES

1. R.V.K., Mangalem, Nirat Ray, Umesh V. Waghmare, A. Sundaresan and C. N. R. Rao, *Solid State Commun., 2009,* ***149****,1.*
2. A. Sundaresan and C. N. R. Rao, *Solid State Communications*, *2009,* ***149,*** *1197.*
3. S. G. bahoosh, S. Trimper and J. Wesselonowa, *Phys. Status Solidi RRL 2011,* ***382****, 10-11.*
4. N. Sharma, A. Gaur and U. Kr Gaur, *Ceramic International 2014,* ***07****, 153.*
5. S. Ramakanth, S. hamad, S. Vanugopal Rao and K. C. James Raju, *AIP Advances, 2015,* ***5,*** *057139.*
6. Tesfakiros Woldu, B. Raneesh, P. Sreekanth, MV Ramana Reddy, Reji Philip and Nandakumar Kalarikkal, *Chem. Phys. Lett.,2015,* ***625****, 58.*
7. M. Bibes and A. basthelemy, *Nat. Mater., 2008,* ***7,*** *425-426.*

8. Anar Singh, Vibhav Pandey, R. K. Kotnala and Dhananjai Pandey, *Phys. Rev. Lett.,2008, **101**, 247602.*
9. Jing Ma., Jiamian HU, Zheng Li and Ce-Wen Nan, *Adv. Mater., 2011, **20**, 1.*
10. M. Fiebig *, J. Phys. D: Appl. Phys.,2005, **38** , R123.*
11. W. Eerenstein and N. D. Mathur , J. F. Scott , *Nature, 2006, **442**, 759.*
12. T. Lottermoser, T. Lonkai, U. Amann, D. Hohlwein, J. Ihringer and M. Fiebig, *Nature, 430 **2004**, 541.*
13. R. O. Cherifi, V. Ivanovaskaya, L. C. Phillips, A. Zobelli, I. C. Infante, E. Jacquet, V. Garcia, S. Fusil, P. R. Briddon, N. Guiblin, A. Mouglin, A. A. Unal, F. Kronast, S. Valencia, B. Dkhil, A. Barthelemy and M. Bibles, *Nat. Mater., 2014, **13**, 345-351.*
14. G. Radaelli, D. Pietti, E. Phekhanov, I. Fina, P. Jorelli, B. R. Salles, M. Cantoni, C. Rinaidi, D. Gutierrez, G. Panaccione, M. varela, S. Picozzi, J. Fontaberta and R. Bertacco, *Nat. commun., 2014, **5,** 3404.*
15. N. Hur, S. Park, P.A. Sharma, J.S. Ahn, S. Guha and S.W. Cheong, *Nature, 2004, **429**,392.*
16. R. Ramesh and N.A. Spaldin, *Nat. Mater., 2007, **6**, 21.*
17. A. Thomasson, S. Chenifi, F. Rowland, B. Guntier, D. Albertini, C. Meny and N. Vjart, J. *Appl. Phys. 2013, **113,** 214101.*
18. M. Glich, I. Fina, A. Moralli, F. sanchez, M. Alaxe, J. Gazquel, J. Fontcubera and A. Roig, *Adv. Mater., 2014, **26,** 4645.*
19. N. A. Hill, *J. Phys. Chem. B, 2000, **104,** 6694.*
20. M. A. Subramanian, T. He, J. Chen, N. S. Rogado, T. G. Calvarese, and A. W. Sleight, *Adv. Mater., 2006, **18** ,1737.*
21. J. H. Park, Hyun M. Jang, Hyung S. Kim, Chan G. Park, and Sang G. Lee, *Appl. Phys. Lett., 2008, **92**, 062908.*
22. S. Valencia, A. Crassous, L. Bocher, V. Garcia, X. Moya, R. O. Cherifi, C. Deranlot, K. Bouzehouane, S. Fusil, A. Zobelli, A. Gloter, N. D. Mathur, A. Gaupp, R. Abrudan, F. Radu, A. Barthélémy and M. Bibes, *Nat., Mater., 2011, **10**, 753.*
23. T. Kimura, Annu Rev Condens *Matt Phys 2012, **3**, 93-110.*
24. B. Raneesh, A.Saha and Nandakumar Kalarikkal, *Radiat. Phys. Chem., 2013, **89,** 28.*
25. L. Ju, T. Sabergharesou, K. G. Stamplecoskie, M. Hegde, T. Wang, N. A. Combe, H. Wu and P. V. Radovanovic, *J. Am. Chem. Soc., 2011, **134** ,1136.*

26. Z. Z. Lazarevic, M. Vijatovic, Z. D. Mitrovic, N. Z. Romcevic, M. J. Romcevic, N. Paunovic and B.D. Stojanovic, *J Eur. Ceram. Soc. 2010, **30**, 623.*
27. Woo-Seok Cho, *J. Phys. Chem. Solids 1998, **59,** 659.*
28. U. Venkateswaran, M. V. Naik and R. Naik, P*hys. Rev. B: Condens. Matt., 1998, **58**, 14256.*
29. Zhou, G. jian, Y. Zheng, S. Gong and F. Shi. *Applied Surface Science 2011, **257,** 7621-7626.*
30. Y. Shiratori, C. Pithan, J. Dornseiffer, and R. Waser, *J. Raman Spectrosc., 2007, **38**, 1288.*
31. D. K. Pradhan, R. N. P. Chowdhray and T. K. Nath, *Appl. Nanosci. 2012, **2**, 261-273.*
32. K.W. Wagner, Ann. Phys. 1993, **40**, 818826.
33. R. S. Devan, Y. D. Kolekarand and B. K. Chougule, *J. Phys: Condens. Matter 2006, **18**, 9809-9821.*
34. R. S. Devan, Y. D. Kolekarand and B. K. Chougule, *J. Alloys Compd. 2008, **461**, 678-683.*
35. A. Gupta and B. Chatterjee, J. Eur. Ceram. Soc. 2013, **33**, 1017-1022.
36. R. Sharma, P. Pahuja and R. P. Tandon, *Ceram. Inter. 2014, **40**, 9027-9036.*
37. A.M. Stoneham, J. Gavartin, A.L. Shluger, A.V. Kimmel, D.M. Ramo, H.M. Ronnow, G. Aeppli and C. Renner, *J. Phys.: Condens. Matter, 2007, **19,** 255208.*
38. J. P. Rivera, *Ferroelectrics, 1994**, 161,** 165*.
39. M. Kumar, A. Srinivas, S. V. Suryanarayana, G. S. Kumar and T. Bhimasankaram, *Bull. Mater. Sci., 1998, **21**, 251.*
40. J. Shah and R. K. Kotnala, *J. Mater. Chem. A, 2013, **1**, 8601.*
41. J. Shah and R. K. Kotnala, *Scr. Mater., 2012, **67**, 316.*
42. S.V. Suryanarayana, *Bull. Mater. Sci. 1994, **17,** 1259.*
43. G. C. Papaefthymiou, *J. Magn. Magn. Mater. 2004, **272**, E1227.*
44. T. J. Park, G.C. Papaefthymiou, A. J. Viescas, A.R. Moodenbaugh and S.S. Wong, *Nano Lett.,2007, **7** , 766.*

Figure captions

Fig. 1: XRD patterns of $BaTiO_3$ samples obtained by varying CA percentage

Fig. 2: XRD pattern of $BaTiO_3$ samples (a) with heat-treatment at different temperatures, and (b) XRD pattern of BT-3 splitting peak (200) and (002) at around $2\theta = 45^0$.

Fig. 3: (a) Grain size versus citric acid percentage and (b) Grain size vs. temperature

Fig. 4: (a) TEM image of sample BT-3, the inset shows 20 nm $BaTiO_3$ nanoparticles, and (b) Lattice image and the inset is a SAED pattern

Fig. 5: Raman spectrum of (a) BT-1 to BT-6 samples, and (b) BT-3 to BT-D samples.

Fig.6: Temperature dependence of dielectric constant (ε') of sample BT-D

Fig. 7: Room-temperature magnetic hysteresis of sample BT-D.

Fig. 8: ME voltage vs. AC magnetic field at constant DC (500 O e) bias magnetic field of $BaTiO_3$ samples.

Fig. 9: ME voltage vs. DC magnetic field at constant AC (5 O e) bias magnetic field of $BaTiO_3$ samples

Fig. 10: Linear ME coefficient vs grain size of $BaTiO_3$ samples

Table caption

Table I. Sample code, CA percentage, calcinations temperature, and grain size and linear magnetoelectric coupling coefficient (α) of respective $BaTiO_3$ samples